Improvement of an annular thin film UV-C reactor by fluid guiding elements

Benedikt Hirt [a],[*], Edgar Hansjosten [b], Andreas Hensel [b], Volker Gräf [a], Mario Stahl [a]

[a] *Department of Food Technology and Bioprocess Engineering, Max Rubner-Institut, Federal Research Institute of Nutrition and Food, Haid-und-Neu-Straße 9, 76131 Karlsruhe, Germany*
[b] *Institute for Micro Process Engineering, Karlsruhe Institute of Technology (KIT), Hermann-von-Helmholtz-Platz 1, 76344 Eggenstein-Leopoldshafen, Germany*

ARTICLE INFO

ABSTRACT

In this paper special elements are inserted into an annular thin film UVC reactor to guide the laminar flow. These "Fluid Guiding Elements" (FGE) divide the flow into three separated laminar currents that are alternatingly directed through a small gap of 0.6 mm facing the UV source by turns. Computational fluid dynamic simulations have been used to visualize the flow dynamics inside the reactor.

The residence time distribution and the Bodenstein number show an increase of back mixing in the reactor with the elements. An Iodide/iodate actinometry comparison has shown a better dose distribution throughout the treated volume based on the FGE. The inactivation of *E. coli* DH5α as an exemplary organism could be improved by more than 4 log levels after 5 passes through the reactor using the FGE independent of the flow rate. The absorbance of a model solution was varied by different dye concentrations and the use of FGE improve the inactivation of *Saccharomyces cerevisiae*.

Industrial relevance: The stabilization of liquid foods before bottling is a crucial aspect. The consumers often do not accept a chemical additive like sulphites in wine or dimethyl carbonate in juices. A physical alternative is the UV-C Treatment. In contrast to a turbulent flow a laminar flow has a far lower pressure drop. Therefore, a lower amount of energy is needed to pump the liquid. This study shows that with fluid guiding elements a sufficient inactivation can be achieved with laminar flow.

1. Introduction

Ultraviolet (UV) treatment of food is a promising technology for the improvement of food safety and the extension of shelf life. It can be an alternative or supplementation to other preservation techniques. Hurdle approaches of UVC in combination with heat (Gouma, Gayán, Raso, Condón, & Álvarez, 2015), high pressure (Sauceda-Gálvez et al., 2020), pulsed electric fields (Noci et al., 2008) and more were investigated and show promising results. Furthermore, it can be used to increase the Vitamin D content of certain foods like mushrooms (Jasinghe & Perera, 2006) or milk (W. Diemair, Janecke, & Ott, 1954). UV treatment is approved for different liquid foods in several countries all over the world (Koutchma, 2018). The US Food and Drug Department (USFDA) and US Department of Agriculture (USDA) [USFDA] for example has concluded that the usage of UV-C light at 253.7nm for food processing is safe and

has further approved its use as an alternative treatment to reduce pathogens (*Escherichia coli* O157:H7, *Listeria monocytogenes*, and Salmonella) and other microorganisms in different juices (FDA, 2000; Abdul Karim Shah, Shamsudin, Abdul Rahman, & Adzahan, 2016). This regulation is only valid for systems of turbulent flow with Reynold numbers higher than 2200 (FDA, 2000). As an emerging nonthermal technology, UV irradiation offers multiple advantages: effective inactivation of a broad range of organisms, minimal loss of nutritional quality of foods, no known toxic effects or residues from the process and a low energy consumption compared to thermal pasteurization.

The wavelength for UV processing ranges from 100 nm to 400 nm. Only the UVC range between 200 nm and 290 nm is called the germicidal range, because here the energy is absorbed by the DNA and RNA (Forney, Moraru, Koutchma, & Tatiana]., 2009). The UV-C light inactivates microorganisms by damaging the nucleic acid. The primary

* Corresponding author.
   E-mail address: Benedik.Hirt@mri.bund.de (B. Hirt).

mechanism of inactivation is the creation of pyrimidine dimers. The thymine (DNA) and cytosine (RNA) dimers change the structure of the nucleic acid and thereby preventing the organisms from replicating.

Depending on the optical properties of liquid foods, the penetration depth of ultraviolet radiation can be low in comparison to drinking water. To overcome this problem different reactor types can be used, e.g. thin film (Pendyala, Patras, Sudhir Gopisetty, & Sasges, 2021), turbulent flow (Rossitto et al., 2012), Taylor Couette (Müller et al., 2017) or Dean vortex reactors (Choudhary et al., 2011; Junqua, Vinsonneau, & Ghidossi, 2020; Müller et al., 2015). A turbulent flow may result in a relatively high pressure drop. A turbulent flow requires a high velocity and therefor reactors have to be longer to deliver the same dose or several passes are necessary. A thin film reactor (TFR) with laminar flow however, shows low radial mixing. The distribution of the UV-C dose within the treated liquid is not as homogenous as with turbulent flow reactors. A thin-film reactor for practical operation has the disadvantage that it is structurally difficult to keep the gap width constant over the reactor length and also particles of the product can clog the gap.

In this study special inserts for a thin film reactor have been tested for their ability to improve the energy transfer into the liquid (Gräf et al., 2017). These special inserts are called fluid guiding elements (FGE) and are built by a selective laser melting technique. It has been shown previously that, if FGE are applied to optimize a pipe-in-pipe heat exchanger, heat transfer can increase greatly in an extent dependent on the reactor length (Hansjosten et al., 2018). Gök et al. (2021) showed in their study that the inactivation of *E. coli DH5α* and *Listeria innocua* in milk can be improved by more than 4 log levels with a dose of close to 4.2 kJ/L with these specific fluid guiding elements.

The aim of this work is to better understand, how the insertion of the fluid guiding elements improves the efficiency of an annular thin-film reactor. Our model conception is based on the fact that the UV energy only penetrates the liquid to a limited extent and is thus attenuated. Therefore, not all the microorganisms are reached and inactivated.

To investigate the change in the characteristics and the back mixing of the thin film reactor due to the insertion of the fluid guiding elements the residence time distribution was determined and the Bodenstein number was calculated. Computational fluid dynamic simulations have been used to visualize the flow dynamics inside the reactor.

The UV-C dose was measured with an chemical iodide/iodate actinometer according to Rahn (1997). to compare differences in the effectivity of the reactor. The inactivation of *E. coli* DHα5 and the far more UV resistant *S. cerevisiae* in a model solution was examined. The absorbance at 254 nm of the model solution was adjusted by varying the concentration of dye.

2. Materials and methods

Unless otherwise described, all chemicals were purchased from Sigma-Aldrich.
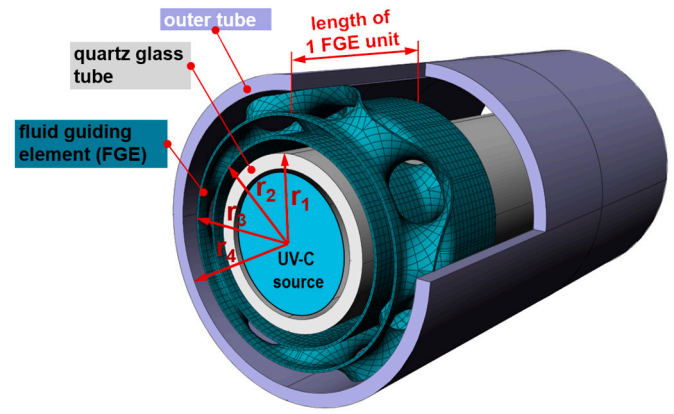

Fig. 1. Schematic illustration of the fluid guiding element inserted into the thin-film reactor. $r_1 = 11.59$ mm; $r_2 = 12.30$ mm; $r_3 = 13.50$ mm; $r_4 = 14.77$ mm; r_2 and r_3 are pointing to the middle of the wall; wall thickness ≈ 0.160 mm; length of one FGE ≈ 60 mm length of one FGE unit ≈ 10 mm.

peak at 253.6 nm wavelength. The quartz tube surrounding the LPM lamp has an outer diameter of about 23.10 mm; the inner diameter of the reactor is about 29.24 mm ("outer tube"). The gap through which the medium flows is 3.06 mm. The luminous length of the lamp is about 344 mm.

The FGE are not mixing the fluid, but dividing the flow stream into three separated laminar currents which are guided alternatingly to the UV lamp. The dimensions of the FGEs are shown in Fig. 1. The gap between the quartz glass tube and the inner wall of the FGE is about 0.63 mm. The length of 1 FGE is about 60 mm. The structure of each FGE consists of 6 units ($l_{unit} = 10$ mm). 8 FGEs are inserted in the reactor.

The Reynolds numbers for the liquid flows inside the three gaps were calculated to classify the flow conditions.

$$Re = \frac{\rho \, d_{hyd}\overline{\omega}}{\eta}$$

Here, ρ is the density, d_{hyd} is the hydraulic diameter, $\overline{\omega}$ is the mean velocity and η is the dynamic viscosity of the fluid. The hydraulic diameter is calculated as

$$d_{hyd} = 4A/P$$

Where A is the cross-sectional area of the flow and P the wetted perimeter of the cross section. In Table 1 all the Reynolds numbers for water at 20°C were shown for the flow rates that were used in the experimental part of this study. Gap 1 is the inner one facing the UV-C source. All Reynolds numbers are well below the critical Reynolds number of 2400 for turbulent flow. This proves a laminar flow in all gaps.

To calculate the flow conditions in an annular thin film the Navier-Stokes equation with cylinder coordinates was used:

$$\rho\left(\frac{\partial \omega_z}{\partial t} + \omega_r \frac{\partial \omega_z}{\partial r} + \frac{\omega_\varphi}{r}\frac{\partial \omega_z}{\partial \varphi} + \omega_z \frac{\partial \omega_z}{\partial z}\right) = -\frac{\partial p}{\partial z} + \eta\left[\frac{1}{r}\frac{\partial}{\partial r}\left(r\frac{\partial \omega_z}{\partial r}\right) + \frac{1}{r^2}\frac{\partial^2 \omega_z}{\partial \varphi^2} + \frac{\partial^2 \omega_z}{\partial z^2}\right] + \rho g_z$$

2.1. Annular UV-C thin-film reactor (TFR) with fluid guiding elements (FGE)

The TFR was developed and constructed in Max Rubner-Institut (MRI) / Department of Food Technology and Bioprocess Engineering as a prototype. The UV-source in the reactor is a 20 W low-pressure mercury (LPM) lamp (UVPro FMD Series) with 7.5 W emitted at its

Assumptions used to simplify the problem were: 1. Steady state; 2. ω_z depends only on r; 3. p depends only on z; 4. Rotational symmetry; 5. No volume force in z-direction. This results in the abbreviated form of the equation:

Table 1

Calculated Reynolds numbers for the thin film reactor with and without fluid guiding elements (FGE) with specific flow rates for water (20°C).

	Reynolds number for the thin film reactor			
	without FGE	with FGE		
Flow L/h		Gap 1	Gap 2	Gap 3
30	203	74	69	63
100	675	247	229	209
150	1013	371	344	313

$$0 = -\frac{\partial p}{\partial z} + \eta \left[\frac{1}{r} \frac{\partial}{\partial r} \left(r \frac{\partial \omega_z}{\partial r} \right) \right]$$

The inner diameter is R and the outer diameter is κR, where κ is the ratio of the outer and inner diameter. Integrating this equation twice and using the boundary conditions $\omega_z(r = R) = 0$; $\omega_z(r = \kappa R) = 0$ yield the equation for the flow profile of the velocity

$$\omega_z = -\frac{\Delta p}{\Delta z} \frac{r^2}{4\eta} \left[1 - \frac{r^2}{R^2} + \frac{1 - \kappa^2}{ln\kappa} ln \left(\frac{R}{r} \right) \right]$$

The unknown term $\frac{\Delta p}{\Delta z}$ is determined by the mean velocity in the gap. The mean velocity is calculated via the flow rate $\dot{V}$ and the flowed-through cross-sectional area.

$$\overline{\omega_z} = -\frac{\Delta p}{\Delta z} \frac{R^2}{8\eta} \left[1 + \kappa^2 + \frac{1 - \kappa^2}{ln\kappa} \right] = \frac{\dot{V}}{A}$$

The flow condition was also investigated with Computational Fluid Dynamics (CFD) with Fluent 6.1. To simplify the problem, only a section of the reactor with an angle of $\varphi = 2°$ was simulated. Further only one of the three paths was simulated, since it is to be expected that they are equal in their flow conditions. In Fig. 3 the velocity of the flow inside the Fluid guiding elements is shown. The contours of the velocity in the middle of each section is also displayed in Fig. 2. The simulated profiles are congruent with the calculated.

To investigate the amount of cross-mixing / the cross-mixing effect the path lines of the fluid inside the FGEs is displayed in Fig. 4. It can be seen that the flow is laminar.

2.2. Residence time distribution

To characterize the performance of the thin film reactor with and without FGEs, residence time distributions (F(t)), mean residence times (τ) and width of the residence time distributions were determined from measured tracer step responses. The step input was imposed by switching the inlet flow from demineralized water to a sodium chloride
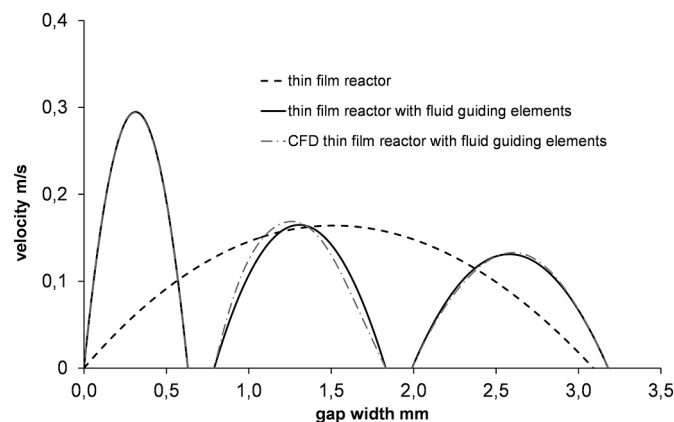
Fig. 2. Calculated flow profile(s) for the thin film reactor and each gap of the fluid guiding elements dependent on the gap width at 100 L/h flow rate in comparison to the CFD simulation of the flow in the Fluid guiding elements.

solution (10 g L^{-1} NaCl, Carl Roth GmbH + Co. KG, Karlsruhe, Germany) containing 0.06% dye (Sunset Yellow FCF) to visualize the entrance of the solution into the reactor at the same time. The conductivity σ(t) measurements started when the colored NaCl solution reached the reactor σ$_0$ (t = 0). σ(t) was measured at the outlet of the reactor by a conductivity sensor (FYA641LFP1, Ahlborn Mess- und Regelungstechnik GmbH, Holzkirchen, Germany) connected to a data logger (Almemo 2690-8A, Ahlborn Mess- und Regelungstechnik GmbH, Holzkirchen, Germany). F(t) was obtained by dividing σ(t) through σ$_{max}$. The residence time distributions were measured in triplicate for the volume flows (30 L/h, 40 L/h 50 L/h, 60 L/h, 70 L/h 80 L/h).

The mean residence time τ was determined by

$$\tau = \int_0^1 t \, dF(t) = \int_0^1 t \, E(t) \, dt$$

Where E(t) is the residence time sum function and F(t) the residence time distribution. F(t) was plotted against the time normalized $\Theta = t/\tau$ by the mean residence time. Each residence time distribution was measured three times.

To evaluate the delay and the axial mixing in the system the Bodenstein number was determined. It characterizes the axial mixing and allows statements whether and how much volume elements or substances within a reactor mix due to the prevalent currents. The dispersion model states that the axial dispersion in a reactor can be described as

$$\frac{\partial c_i}{\partial t} = D_{ax} \frac{\partial^2 C_i}{\partial z^2} - \overline{\omega} \frac{\partial c_i}{\partial z} \tag{3}$$

With the axial dispersion coefficient D_{ax} and the average flow velocity $\overline{\omega}$ in z-direction. Since the reactor is open on both ends, this differential can be solved analytically to

$$E(Bo) = \frac{1}{2} \sqrt{\frac{Bo}{\pi \cdot \Theta}} \cdot exp \left(-\frac{(1 - \Theta)^2 Bo}{4\Theta} \right) \tag{4}$$

To determine the Bodenstein number the solver Function of Excel was used to minimize the sum of the errors squared between $E(t)$ and $E(Bo)$ by varying the Bodenstein number. One Bodenstein number was fitted for $E(\theta \leq 1)$ and one for $E(\theta > 1)$ according to Fitzer, Fritz, and Emig (1995). The mean and standard deviation of the six Bodenstein number of each triplet was calculated.

2.3. Actinometry

The UV-C energy absorbed by the liquid is based on specific system parameters, such as flow patterns and reactor geometry. The dose of UV-radiation was determined by the chemical iodide/iodate actinometer developed and described by Rahn (1997). This is the most commonly used chemical actinometer to measure the dose delivered in flow-through UV-C reactors (Junqua et al., 2020).

This is a chemical reaction (Eq.3) in which a potassium iodide-iodate solution forms photochemical product as triiodide upon absorption of UV-C photons. The reaction is as follows:

$$8 \, KI + KIO_3 + 3 \, H_2O + h\nu \rightarrow 3 \, I_3^- + 6 \, OH^- + 9 \, K^+ \tag{5}$$
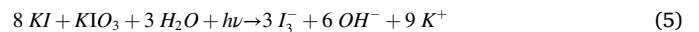
Irradiation results in the linear formation of triiodide, which is quantified by measuring its absorbance at 352 nm. The UV-C dose can then be determined by linear regression. A solution of 0.6 M iodide and 0.1 M iodate in 0.01 M borate buffer (pH 9.25) was used as a chemical actinometer to measure the UV-C dose at 254 nm in different passes. The aqueous solution is optically opaque to radiation below 290 nm and absorbs all of the germicidal wavelengths. With this method, it is possible to determine the amount of energy the solution has absorbed. The UV-C dose (D_{act} in J L^{-1}) was calculated using the following equation:

$$D_{act} = \frac{A_{352\ nm} \cdot P_{253.7\ nm}}{pl \cdot \phi \cdot \varepsilon_{352\ nm}} \qquad (6)$$

where $A_{352\ nm}$ is the measured absorbance at 352 nm, $P_{253.7\ nm}$ the number of joules per Einsteins of 253.7 nm photons (4.716×10^5 J einst^{-1}), pl is the path length of the cuvette (1 cm), ϕ is the quantum yield (effects per photon in mol einst^{-1}), and $\varepsilon_{352\ nm}$ is the molar absorption coefficient of triiodide at 352 nm (27,600 dm^3 mol^{-1} cm^{-1}). A basic value of 0.73 and its temperature and concentration dependence was applied as quantum yield:

$$\phi = 0.73 \times (1 + 0.23 \times [c_i - 0.577]) \times (1 + 0.02 \times [T_i - 20.7°C]) \qquad (7)$$

where c_i is the concentration of the iodide ($A_{300\ nm} \times 1.061^{-1}$) and T_i is the temperature in °C. Samples were taken before treatment (control) and after each pass. Samples were measured at 352 nm and to determine the quantum yield, the control was measured photometrically at 300 nm (Spectrometer UNICAM UV2 UV/VIS).

2.4. Standard operating procedure for UV-C treatment with a TFR

The standard operating procedure was applied for the microbiological inactivation as well as for the actinometry. To ensure stable lamp performance the UV-C lamps were switched on 45 min prior to the experiment. During this phase water with 20°C was pumped through the reactor to cool the reactor and to verify the flow rate (measuring volume of pumped water by time).

The experimental solution was stored in a sterile bottle and tempered at 20°C. The tube of the feeding peristaltic pump (Heidolph Hei-FLOW Precision 06) was sterilized with Bacillol® before pumping solution through the reactor. The first 150–200 mL emerging the reactor were discarded. At this point a steady state was reached. Approximately 50 mL were sampled from the stream while the reactor was in steady state. The remaining solution was collected in a sterile bottle and was then used as the new feeding solution. This process was repeated for each pass.

After the experiments the reactor was cleaned following this procedure: First 2 L of demineralized water was pumped through the reactor. Then a 70% ethanol solution was pumped in circulation for about 10 min. The reactor was then flushed again with 2 L demineralized water. At the end the reactor was blown dry with compressed air. The lamps are being kept on during the cleaning process. At regular intervals the reactor is additionally cleaned with a 0.1 Mol NaOH solution.

2.5. Investigation of microbial inactivation

Escherichia coli DH5α was grown in standard nutrient broth 1 by shaking at 90 rpm on a shaking incubator for 18 h at 37°C. The nutrient broth with *E. coli* was centrifuged and decanted. The *E. coli* was inoculated into Ringer solution. An equal amount of nutrient broth and Ringer solution results in a concentration of approximately 10^8 CFU/ml. *Saccharomyces cerevisiae* (EATON SIHA®, strain D 576) was incubated at 30°C for 24 h at 90 rpm in YPM broth. The Ringer solution was inoculated with 10^6 CFU/ml. The absorbance of the solution was adjusted with the food dye sunset yellow (SY). The solutions were treated with UV-C energy at different flow rates with and without FGEs inserted into the TFR. For each assay, the inoculated liquid was completely pumped through the reactor. The initial cell counts (before UV-C inactivation) were determined and samples were taken after each pass through the system and UV-C treatment. In order to determine microbial counts, the UV-C treated medium was diluted in tenfold dilution series in 0.9% NaCl and plated out on Standard nutrient agar 1. In order to obtain a low detection limit, 1 mL volumes of undiluted samples were also plated. Agar plates with *E. coli* were incubated at 37°C for 24 h. Agar plates with *S. cerevisiae* were incubated at 30°C for 48 h. Then colonies were

counted. All microbial count determinations were done in triplicate and the mean of triplicate determinations was calculated.

Microorganisms in foods exposed to UV-C treatments can exhibit different inactivation behaviors. The behavior be described by a log-linear, linear with tailing, sigmoidal-like, linear with shoulder, biphasic types of curves etc. The inactivation kinetics of microorganisms depend on the type of microorganisms (bacteria, yeasts, molds etc.)

2.6. Physical properties of the used liquids

The physical properties of the liquids are important factors influencing the efficiency of the UV-C treatment. Flow properties are based on viscosity and density. How many organisms are reached by UV-C light depends on the optical properties of the liquid. The extinction measured before and after inoculation. The extinction of a solution is called absorbance A. The extinction of a dispersion is called optical density OD. In this paper the term absorbance is only used for effect of the dye sunset yellow (SY) and therefore the liquid before inoculation. The term OD describes the extinction of the solution after inoculation with microorganisms. Relevant physical properties of the investigated liquids are reported in Table 2. The observed turbidity is only caused by the microorganisms themselves. The turbidity was measured with a Turbiquant® 3000 IR from the company Merck KGaA.

3. Results and discussion

3.1. Reactor characterization

To evaluate the performance of the UV-C reactor and enable comparisons to other reactors the residence time distributions (RTD) were measured with and without FGEs. The RTD can further show the change in the reactor characteristics caused by the insertion of the FGEs. The mean residence time of the TFR is shorter with FGEs because the insertion of FGEs into the reactor causes a reduction of the reactor volume. To enable a comparison between the two setups, the residence time is normalized by the mean residence time. Fig. 5 shows the RTD for the TFR with and without the FGEs for the 3 flow rates used for the inactivation in 3.3.

The residence time distribution in the TFR is narrower with FGEs. There is a lot more tailing without the FGE. It takes about 4 times the mean residence time before the concentration reaches 100%. Where the reactor with FGE reaches the 100% concentration before 2τ. There is no dependence on the flowrate of the RTD of the reactor without FGEs. The flow conditions stay the same. This is reflected by the almost identical Bodenstein numbers (Table 3). The fits for F(Bo) are not able to reproduce the tailing of F(t). The Dispersion model reached its limit, because the reactor acts almost like a laminar tube flow.

The model fits for the TFR with FGE. The Bodenstein numbers reflect the change in the RTD due to the flow rate.

Fig. 5 shows a comparison of the Bodenstein number of the thin film reactor with and without the FGEs. The insertion of the FGEs into the reactor raises the Bodenstein numbers (Table 3). This indicates that there is less axial mixing within the reactor with FGEs.

The reactor volume can be calculated with the mean residence time for each flow rate. The mean volume for the TFR is $147,5 \pm 7, 1\ cm^3$. With the insertion of the FGEs the volume is reduced to $120,8 \pm 6, 2\ cm^3$. The reduction is by $18, 1 \pm 5, 8\%$.

3.2. Actinometric investigation of the reactor

To estimate the effect of hydraulic characteristics on the energy absorption of the liquid, the UV-C energy input by iodide/iodate actinometry was determined in triplets at different flow rates with and without fluid guiding elements (FGE).

To determine the actinometric dose, the Iodide/Iodate solution was treated in 3 passes through the reactor. Fig. 3 shows the results of the

Table 2
Physical properties of the used liquids.

Properties	$A_{254,\,1cm}$ [−] without organisms	$OD_{254nm,1cm}$ [−]	turbidity [NTU]	dynamic viscosity η [mPa*s] at 20°C	density ρ [g/cm³] at 20°C
Ringer's solution +0.06% SY + *E. coli* DH5α (10⁸ CFU/ml)	21.0 ± 3.0	28.6 ± 2.2	270.0 ± 28.7	1.06 ± 0.02	1.00 ± 0.01
Ringer's solution + *Saccharomyces cerevisiae* (10⁶ CFU/ml)	0	0,1 ± 0.1	16,5 ± 0.1	1.04 ± 0.01	n.m.
Ringer's solution +0.03% SY + *S. cerevisiae* (10⁶ CFU/ml)	12.1 ± 1.1	12,3 ± 0.9	16.2 ± 1.7 17.7 ± 2.1	1.04 ± 0.02	n.m.
Ringer's solution +0.07% SY + *S. cerevisiae* (10⁶ CFU/ml)	29.2 ± 1.7	29.5 ± 2.1	17.1 ± 1.1 17.9 ± 2.3	1.03 ± 0.02	n.m.
actinometric solution	179.0 ± 1.7	–	0 ± 0.1	1.02 ± 0.01	1.08 0.01

Table 3
Comparison of the mean residence time and the Bodenstein number of the TFR with and without FGE at different flow rates.

	TFR without FGE		TFR with FGE	
Flow [L/h]	τ_{TFR} [s]	Bo	$\tau_{TFR+FGE}$ in [s]	Bo
30	16.80 ± 1.51	17 ± 4	13.53 ± 0.42	24 ± 1
40	12.73 ± 0.31	23 ± 8	10.50 ± 0.14	30 ± 9
50	10.30 ± 0.12	22 ± 7	8.50 ± 0.12	27 ± 2
60	8.60 ± 0.01	22 ± 6	7.20 ± 0.01	28 ± 2
70	7.20 ± 0.01	24 ± 6	6.50 ± 0.31	29 ± 2
80	6.30 ± 0.47	23 ± 8	5.90 ± 0.23	40 ± 8
100	5.46 ± 0.09	20 ± 3	4.93 ± 0.09	60 ± 4
150	3.66 ± 0.19	19 ± 4	3.33 ± 0.19	72 ± 9

averaged actinometric dose and its deviations for the three flow rates (30 L/h, 100 L/h and 150 L/h) that were used for the microbiological inactivation. The actinometric dose increases linear with the numbers of passes through the reactor. This shows that the reagents are not depleted in the solution as a whole. (See Fig. 6).

It is worth mentioning, that the multi-pass approach is in some ways similar to improving mixing. For each pass the low dose fluid elements are mixed with the high-dose ones.

The actinometric dose is shown in comparison to the theoretically calculated UV-C energy input $D_{th.max} = P_{UV}/\dot{V}$ (Fig. 7). The emitted power of the UV-C source at 254 nm is 7.5 W according to the manufacturer's specification. The difference between the actinometric dose and the theoretical maximal dose at low flow rates exists due to the fact that the penetration depth of the UV light into the solution is so small that only the surface area facing the UV-lamp is treated. Rahn et al. (2003) showed that the quantum yield decreaces by about 6% when the iodide concentration decreases from 0.6 Mol to 0.1 Mol. If the concentration decreases further the quantum yield drops very low. This is locally the case for the portion of the soultion facing the lamp. UV light is absorbed by the solution without generating new tri-iodide. The TFR with FGE is closer to the theoretical dose. The FGE direct 3 different elements of flow in the proximity of the UV lamp. At high flow rates the
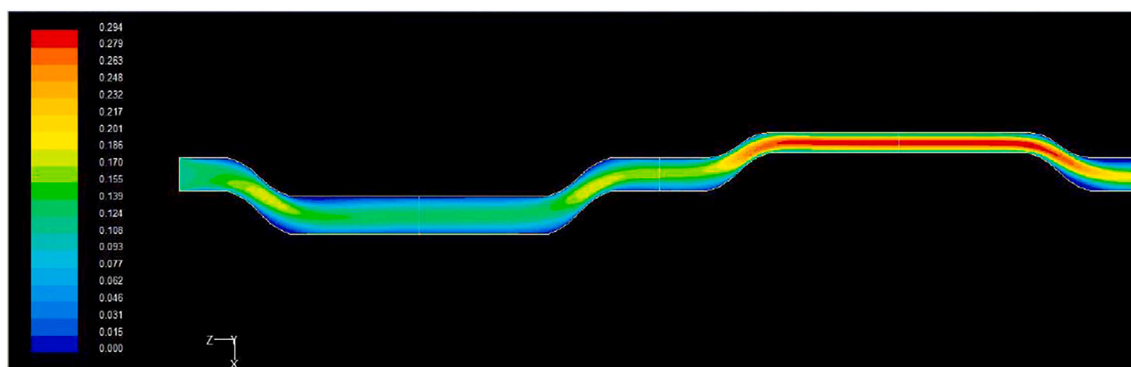

Fig. 3. CFD Simulation of the flow velocity in the fluid guiding elements.
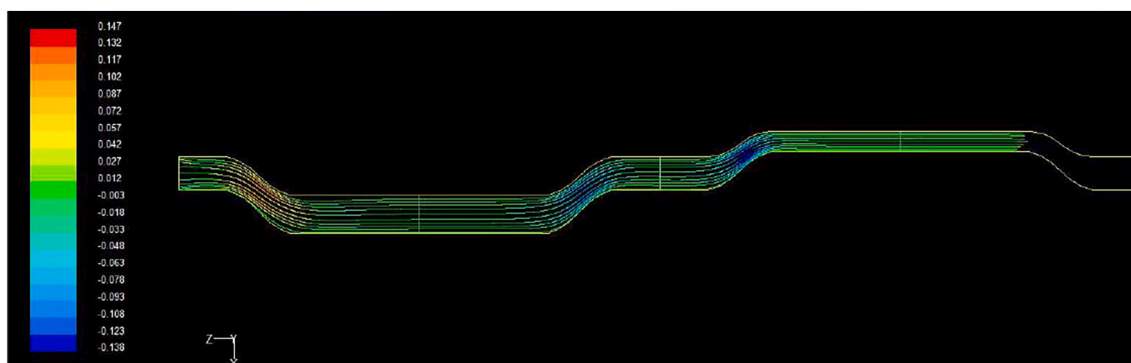

Fig. 4. CFD simulated path lines of the flow inside the fluid guiding elements and their axial velocity.
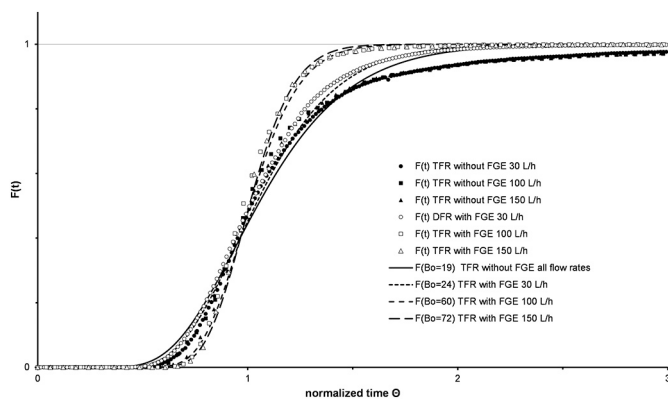
Fig. 5. Residence time distribution in the thin film reactor with and without fluid guiding elements normalized by the mean residence time for flowrates of 30 L/h, 100 L/h and 150 L/h. The respective Bodenstein-models are plotted. To keep the illustration lucid, the Bodenstein number for the TFR without FGE were averaged and only one graph was plotted.
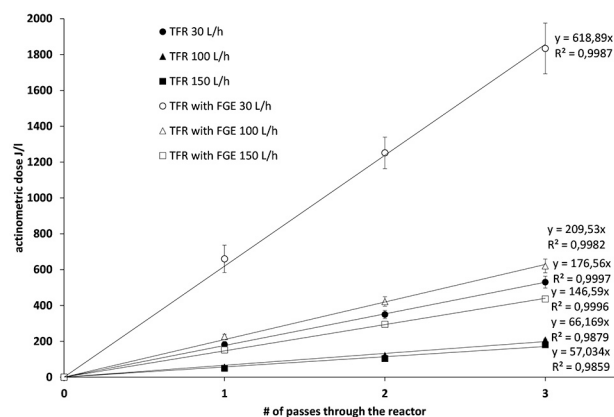

Fig. 6. Actinometric dose measurements for each flow rate in the TFR with and without the fluid guiding elements.
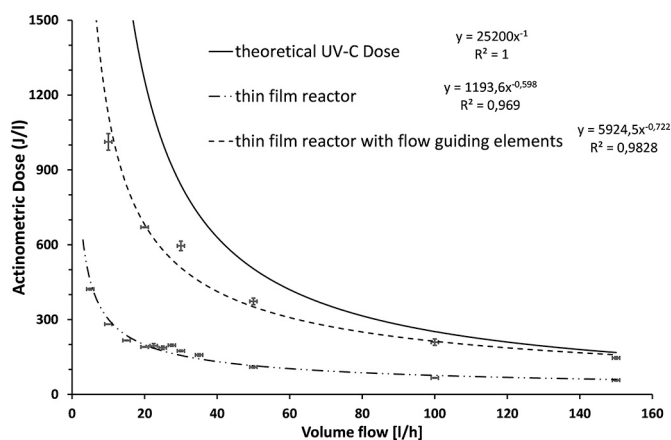

Fig. 7. Comparison of the actinometric dose of the thin film reactor with and without fluid guiding elements and the theoretical maximal dose depending on the flow.

actinometric dose of the TFR with FGE is almost identical to the theoretical one. The residence time in the reactor is shorter. Therefore, the reaction's quantum yield limit is not exceeded. The high absorbance of the actinometric solution causes a low penetration depth. It can be

assumed that all of the UV-C radiant power of the mercury-low pressure-lamp is absorbed by the solution. The difference between the actinometric dose and the theoretical one shows that not all of the radiant power is measured. Especially at long exposure times the actinometry is reaching its limit and the actinometric dose can not represent the actual UV dose absorbed by a liquid medium in the reactor. The theoretical UV-C dose is calculated with the manufacturer specification of 7.5 W radiation at 254 nm. This specification is valid for the ideal temperature for this UV Pro N20-2 mercury-low-pressure-lamp of 21–25°C (specification sheet). The actual emitted UV-C power is dependent on the temperature as well as the cumulative operation time of the lamp.

This shows that the iodide/iodate actinometry is not viable to measure the total power of energy absorbed by a liquid in the reactor with laminar flow. Rather, the results give insight in the non-uniformity of the absorbed energy. This nonuniformity can be shown by the calculated dose distribution in the gap. The decrease of irradiance can be calculated with the Beer-Lambert law (Fig. 8 left).

$$I(r) = I_0 \cdot \frac{r_0}{r} \cdot 10^{-A \cdot (r - r_0)}$$

With the flow velocity $\omega(r)$ dependent on the radius of the reactor, A the decadic absorbance and the reactor length l the residence time $t(r)$ can be calculated. With the Irridiance distribution the dose distribution can be calculated:

$$D = I(r) \cdot t(r) = I(r) \cdot \frac{\omega(r)}{l}$$

This calculated dose distribution is shown in Fig. 8 (right) for the actinometric solution as well as for the model solutions used for the inactivation experiments in the TFR with FGE at 100 L/h.

This calculation can also show how much dose was absorbed by a partial volume dependent on the residence time. In Fig. 9 the UV-dose distribution for a model solution with an optical density of 12.3 is plotted over the normalized time. The partial volumes coming simultaneously out of the reactor were either facing the lamp or the outer reactor wall which results in different doses. At the outlet of the reactor the averaged dose distribution (displayed in Fig. 9) would be observed.

Koutchma, Keller, Chirtel, and Parisi (2004) established a biodosimetric method to measure this dose distribution in combination with residense time distribution by injecting E.coli K12 into the feeding stream as a tracer (Fenoglio, Ferrario, García Carrillo, Schenk, & Guerrero, 2020; Kaya & Unluturk, 2016). However, this method is not viable with the given residence times of the TFR.

3.3. Efficiency of thin-film reactor with and without fluid guiding elements

The efficiency of the system was also investigated using biodosimetry with the model organism *E. coli* DH5α as a further method to evaluate UV-C energy input. Using the food colorant Sunset yellow FCF, absorbance at 254 nm was adjusted to 28.3 ± 2.2. The inactivation of *E. coli* in a Ringer solution colored with sunset yellow in a TFR improves multiple orders of magnitude when FGEs are inserted. The inactivation of *E. coli* DH5α is dependent on the number of passes through the reactor as shown in Fig. 10. The inactivations without the FGE do not show any significant difference (ANOVA-Test). Analougus to the actinometric investigations only the organisms in the part of the solution facing the lamp are inactivated. The inactivation with FGE 100 L/h and 150 L/h show no significant difference. The inactivation with FGE at 30 L/h works slightly better due to the longer residence time and therefor higher theoretical UV dose of 840 J/L. The same inactivation curves as in Fig. 10 show no dose-response relationship to the theoretical dose caused by different flow rates (Fig. 11).

The treated portion of the solution in proximty to the UV-source does not get interchanged. There is next to no axial mixing in laminar flow. Similar to the actinometry there seems to be a layer thickness in which the UV-light inactivates the *E. coli* population regardless of the
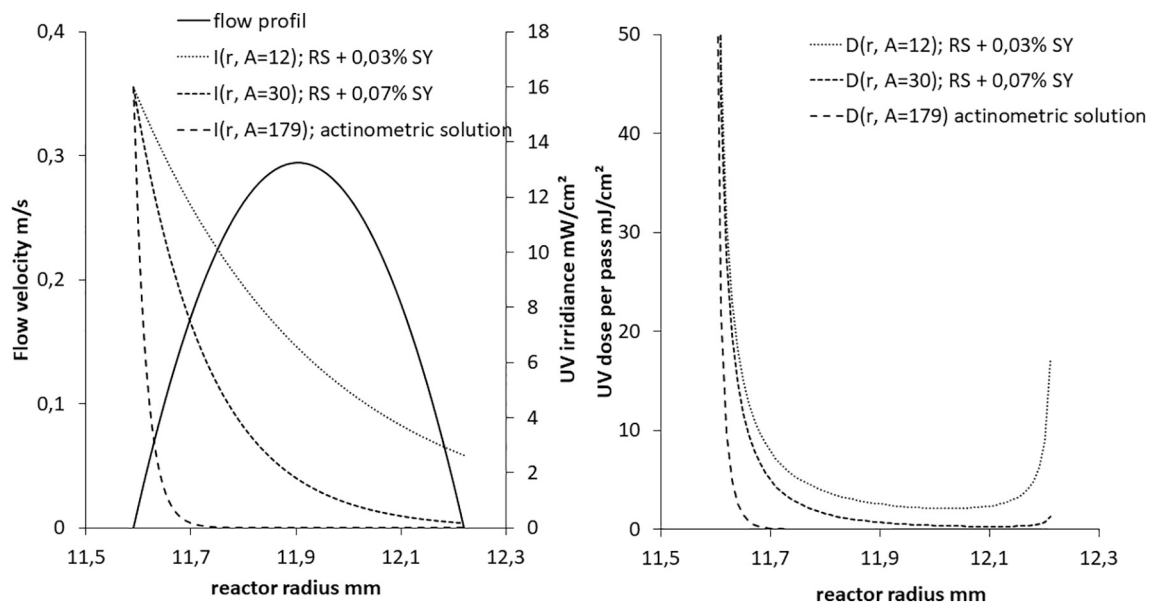
Fig. 8. UV-irradiance distribution (left) and UV-C dose distribution (right) within annular UV-reactor with FGE of radius 11,59 mm and a gap of 6 mm at 100 L/h for absorbances of 12, 30 and 179.
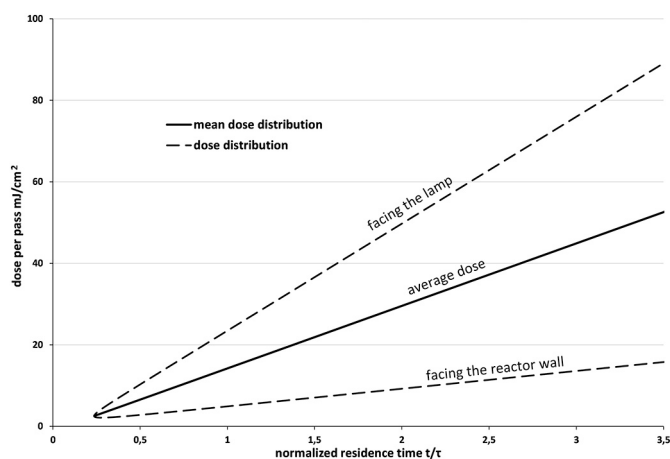

Fig. 9. Theoretical UV-Dose distribution dependent on the residence time for the thin film reactor with fluid guiding elements and a model solution with an optical density of 12.3.

Fig. 10. Effect of Fluid Guiding Elements (FGE) on the inactivation of *E. coli* DH5α in Ringer Solution with 0.06% Sunset at 30 L/h, 100 L/h and 150 L/h plotted against the number of passes through the reactor with 10^8 initial microbial loads. Values are given as means ($n = 3$) $\pm$ standard deviation. *OD* ($254 nm; 1 cm$) $= 28, 3 \pm 2, 2$.

difference in the studied residence times. The inactivation shows a tailing or a convex curve. This is similar to the resuls shown by Murakami, Jackson, Madsen, and Schickedanz (2006) for *E.coli K12*, where a biphasic curve with a tailing was observed. Other studies however found log-linear curves for the inactivation of other *E. coli* strains. Bhullar et al. (2018) for example invastigated the *Escherichia coli ATCC 25922* and found a log-linear inactivation. It can be ruled out, that the reason of the observed tailing is based on the rector design, since the inactivation of *S. cervisiae* for example shows no such behavior.

E. coli Dh5α is known to be very sensitive to UV light. Therefore, the inactivation efficiency of the TFR with FGEs was also investigated with the more UV resistant *Saccharomyces cerevisiae* with an initial load of 10^6 CFU/ml in the model solution.

Inactivation was measured at 100 L/h. The absorbance of the model solutions was set to values of about 0, 10 (0.03% sunset yellow) and 30 (0.07% sunset yellow). The results are shown in Fig. 12. It is obvious that the inactivation curve of the *S. cerevisiae* D 576 shows a complete different characteristic than the *E. coli* Dh5α. The inactivation of *S. cerevisiae* shows a convex/shoulder. Sommer, Haider, Cabaj,
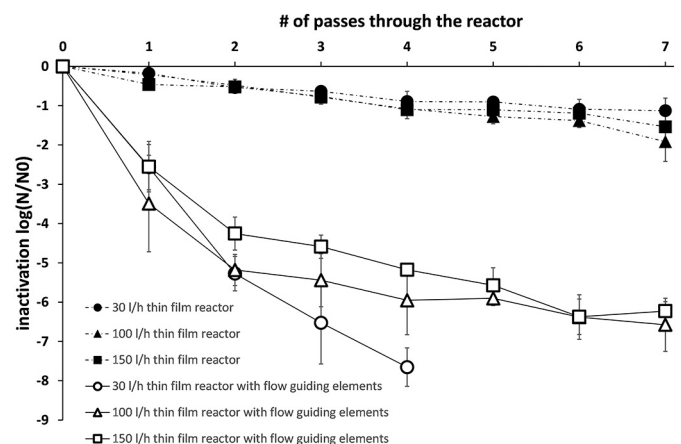
Heidenreich, and Kundi (1996) studied the inactivation of Saccharomyces and found strains (RC43a and a wild type) that show a similar shoulder comparable to the observed D576. They also found strains with a log-linear inactivation (YNN281 and YNN282). Junqua et al. (2020) studied the inactivation of *S. cerevisiae* FX10 in wine and also detected a shoulder in the inactivation curve. Feliciano, Estilo, Nakano, and Gabriel (2019) observed a similar convex characteristic for *S. cerevisiae* BFE-39 in orange juice The inactivation for the solutions without the addition of sunset yellow (OD $= 0.1 \pm 0.1$) deteriorates by insertion of the FGEs. The penetration depth exceeds the thickness of the thin film layer and the walls of the FGEs are hindering the penetration of the UV-C light. As soon as there is an absorbing liquid, the inactivation is enhanced by the FGEs. With an absorbance of 11.7 ± 1.4 there is a 5-log reduction after 4 passes through the reactor in comparison to an only 1.4 log reduction with the common TFR with an optical density of $12,7 \pm 1,2$ after 5 passes. The inactivation of 1.4 log levels is also achieved with the FGEs and the optical density of 30.4 ± 2.3 of the solution. Only 0.3 log level
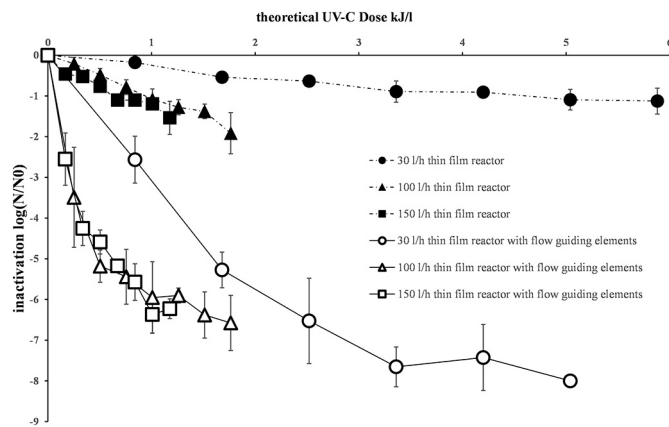
Fig. 11. Inactivation of *E. coli* in Ringer Solution with 0.06% Sunset Yellow with a UV TFR with and without fluid guiding elements at 30 L/h, 100 L/h and 150 L/h plotted against the maximal theoretical UV Dose. A $(254nm; 1cm) = 28, 3 \pm 2, 2$. (For interpretation of the references to colour in this figure legend, the reader is referred to the web version of this article.)
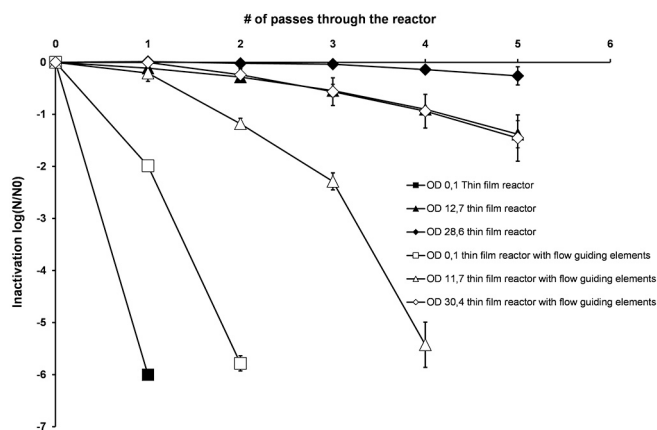

Fig. 12. Effect of fluid guiding elements (FGE) on the inactivation kinetics of *Saccharomyces cerevisiae* in a model solution with different optical densities at 100 L/h with 10^6 CFU/ml initial microbial load. Values are given as means ($n = 3$) $\pm$ standard derivation.

reduction is achieved with the TFR without FGEs with an absorbance of 28.6 ± 1.7. These results confirm the findings with *E. coli*, that the inactivation in a thin film reactor can be significantly improved with the insertion of fluid guiding elements for liquids with an absorbance of at least 10.

4. Conclusions

This study shows that the distribution of UV-C light throughout optically absorbing liquids with a common thin film reactor can be drastically increased by inserting Fluid Guiding Elements (FGE). The actinometric dose measurements show that the FGEs successfully exchange the flow layers facing the energy input of the UV-C source. The width of the residence time distribution becomes narrower with the insertion of the FGEs indicated by the Bodenstein number. Therefore, the UV-C dose is distributed more homogeneously through the treated medium.

The effect of an even distribution throughout the medium is visible in the inactivation of *E. coli* and *S. cerevisiae*. When treated in a thin film reactor with fluid guiding elements the inactivation of *E. coli* in a model solution (A = 28.3) is 4 log levels higher than without the FGE insertions. The inactivation is not connected to the examined flow rates in

laminar flow conditions. Therefore, the inactivation is also independent of the dose measured by the actinometric system. It is rather dependent on the number of passes through the reactor. That is due to the fact that there is little mixing in laminar flow.

The shown improvements of the UV-C reactors proved successful for the UV-C sensitive *E. coli* are as well as for the more resistant *S. cerevisiae*. The inactivation of *S. cerevisiae* with different absorbances shows that the use of fluid guiding elements with a 0.6 mm gap is especially useful for optically absorbing fluids. The gap of the fluid guiding elements should be fitted for future applications to the absorbance level of the treated liquid.

To summarize the results, FGE considerably improve the efficiency of annular thin film reactors.

CRediT authorship contribution statement

Benedikt Hirt: Writing – original draft, Formal analysis, Visualization, Investigation, Conceptualization, Project administration. **Edgar Hansjosten:** Methodology, Conceptualization, Resources. **Andreas Hensel:** Writing – review & editing, Conceptualization, Resources. **Volker Gräf:** Writing – review & editing, Conceptualization, Funding acquisition. **Mario Stahl:** Writing – review & editing, Funding acquisition, Supervision, Conceptualization.

Declaration of Competing Interest

All authors declare that they do not have any conflict of interest.

References

Abdul Karim Shah, N., Shamsudin, R., Abdul Rahman, R., & Adzahan, N. (2016). Fruit juice production using ultraviolet pasteurization: A review. *Beverages, 2*(3), 22. https://doi.org/10.3390/beverages2030022

Bhullar, M. S., Patras, A., Kilanzo-Nthenge, A., Pokharel, B., Yannam, S. K., Rakariyatham, K., … Sasges, M. (2018). Microbial inactivation and cytotoxicity evaluation of UV irradiated coconut water in a novel continuous flow spiral reactor. *Food Research International (Ottawa, Ont.), 103*, 59–67. https://doi.org/10.1016/j.foodres.2017.10.004

Choudhary, R., Bandla, S., Watson, D. G., Haddock, J., Abughazaleh, A., & Bhattacharya, B. (2011). Performance of coiled tube ultraviolet reactors to inactivate Escherichia coli W1485 and Bacillus cereus endospores in raw cow milk and commercially processed skimmed cow milk. *Journal of Food Engineering, 107*(1), 14–20. https://doi.org/10.1016/j.jfoodeng.2011.06.009

Diemair, W., Janecke, H., & Ott, D. (1954). Der Einfluß der UV-Bestrahlung auf die Inhaltsbestandteile der Milch. *Fresenius' Zeitschrift für analytische Chemie, 143*(5), 354–360. https://doi.org/10.1007/BF00440987

Feliciano, R. J., Estilo, E. E. C., Nakano, H., & Gabriel, A. A. (2019). Ultraviolet-C resistance of selected spoilage yeasts in orange juice. *Food Microbiology, 78*, 73–81. https://doi.org/10.1016/j.fm.2018.10.003

Fenoglio, D., Ferrario, M., García Carrillo, M., Schenk, M., & Guerrero, S. (2020). Characterization of microbial inactivation in clear and turbid juices processed by short-wave ultraviolet light. *Journal of Food Processing and Preservation, 44*(6). https://doi.org/10.1111/jfpp.14452. e14452.

Fitzer, E., Fritz, W., & Emig, G. (1995). *Technische Chemie: Einführung in die Chemische Reaktionstechnik (Vierte, vollständig überarbeitete und erweiterte Auflage)*. Springer Berlin Heidelberg: Springer-Lehrbuch. https://doi.org/10.1007/978-3-662-10229-9

Forney, L. J., Moraru, C. I., Koutchma, T., & [Tatiana].. (2009). *Ultraviolet light in food technology*. CRC Press. https://doi.org/10.1201/9781315112862

Gök, S. B., Vetter, E., Kromm, L., Hansjosten, E., Hensel, A., Gräf, V., & Stahl, M. (2021). *Inactivation of E. coli and L. innocua in milk by a thin film UV-C reactor modified with flow guiding elements (FGE)*. Advance online publication. https://doi.org/10.1016/j.ijfoodmicro.2021.109105.

Gouma, M., Gayán, E., Raso, J., Condón, S., & Álvarez, I. (2015). Inactivation of spoilage yeasts in apple juice by UV–C light and in combination with mild heat. *Innovative Food Science & Emerging Technologies, 32*, 146–155. https://doi.org/10.1016/j.ifset.2015.09.008

Gräf, V., Kromm, L., Hensel, A., Hansjosten, E., Gomez, M., Stahl, M., & Greiner, R. (2017). Improving UV-C treatment of liquids in a thin film reactor using flow conducting elements. In *31st EFFoST international conference, 13–16 November 2017, Melia Sitges, Spain*. https://www.openagrar.de/receive/openagrar_mods_00032927.

Hansjosten, E., Wenka, A., Hensel, A., Benzinger, W., Klumpp, M., & Dittmeyer, R. (2018). Custom-designed 3D-printed metallic fluid guiding elements for enhanced heat transfer at low pressure drop. *Chemical Engineering and Processing, 130*, 119–126.

Irradiation in the Production. (2000). Processing, and handling of food 71056. https://www.federalregister.gov/documents/2000/11/29/00-30453/irradiation-in-the-production-processing-and-handling-of-food.

Jasinghe, V. J., & Perera, C. O. (2006). Ultraviolet irradiation: The generator of vitamin D2 in edible mushrooms. *Food Chemistry, 95*(4), 638–643. https://doi.org/10.1016/j.foodchem.2005.01.046

Junqua, R., Vinsonneau, E., & Ghidossi, R. (2020). Microbial stabilization of grape musts and wines using coiled UV-C reactor. *OENO One, 54*(1), 109–121. https://doi.org/10.20870/oeno-one.2020.54.1.2944

Kaya, Z., & Unluturk, S. (2016). Processing of clear and turbid grape juice by a continuous flow UV system. *Innovative Food Science & Emerging Technologies, 33*, 282–288. https://doi.org/10.1016/j.ifset.2015.12.006

Koutchma, T. (2018). Status of international regulations for ultraviolet treatment of foods. *IUVA News 2018, 20*(2). https://uvsolutionsmag.com/iuva-archive/.

Koutchma, T., Keller, S., Chirtel, S., & Parisi, B. (2004). Ultraviolet disinfection of juice products in laminar and turbulent flow reactors. *Innovative Food Science & Emerging Technologies : IFSET : The Official Scientific Journal of the European Federation of Food Science and Technology, 5*(2), 179–189. https://doi.org/10.1016/j.ifset.2004.01.004

Müller, A., Günthner, K. A., Stahl, M. R., Greiner, R., Franz, C. M., & Posten, C. (2015). Effect of physical properties of the liquid on the efficiency of a UV-C treatment in a coiled tube reactor. *Innovative Food Science & Emerging Technologies, 29*, 240–246. https://doi.org/10.1016/j.ifset.2015.03.018

Müller, A., Orlowska, M., Knörr, M., Stahl, M. R., Greiner, R., & Koutchma, T. (2017). Actinometric and biodosimetric evaluation of UV-C dose delivery in annular, Taylor-Coutte and coiled tube continuous systems. *Food Science and Technology International = Ciencia Y Tecnologia De Los Alimentos Internacional, 23*(3), 222–234. https://doi.org/10.1177/1082013216679010

Murakami, E. G., Jackson, L., Madsen, K., & Schickedanz, B. (2006). Factors affecting the ultraviolet inactivation of Escherichia coli K12 in Apple juice and a model system. *Journal of Food Process Engineering, 29*(1), 53–71. https://doi.org/10.1111/j.1745-4530.2006.00049.x

Noci, F., Riener, J., Walkling-Ribeiro, M., Cronin, D. A., Morgan, D. J., & Lyng, J. G. (2008). Ultraviolet irradiation and pulsed electric fields (PEF) in a hurdle strategy for the preservation of fresh apple juice. *Journal of Food Engineering, 85*(1), 141–146. https://doi.org/10.1016/j.jfoodeng.2007.07.011

Pendyala, B., Patras, A., Sudhir Gopisetty, V. V., & Sasges, M. (2021). UV-C inactivation of microorganisms in a highly opaque model fluid using a pilot scale ultra-thin film annular reactor: Validation of delivered dose. *Journal of Food Engineering, 294*, 110403. https://doi.org/10.1016/j.jfoodeng.2020.110403

Rahn, R. O. (1997). *Potassium iodide as a chemical actinometer for 254 nm radiation: Use of Iodate as an electron scavenger*.

Rahn, R. O., Stefan, M. I., Bolton, J. R., Goren, E., Shaw, P.-S., & Lykke, K. R. (2003). Quantum yield of the iodide-iodate chemical actinometer: Dependence on wavelength and concentrations. *Photochemistry and Photobiology, 78*(2), 146–152. https://doi.org/10.1562/0031-8655(2003)078<0146:qyotic>2.0.co;2

Rossitto, P. V., Cullor, J. S., Crook, J., Parko, J., Sechi, P., & Cenci-Goga, B. T. (2012). Effects of UV irradiation in a continuous turbulent flow UV reactor on microbiological and sensory characteristics of cow's milk. *Journal of Food Protection, 75*(12), 2197–2207. https://doi.org/10.4315/0362-028X.JFP-12-036

Sauceda-Gálvez, J. N., Tió-Coma, M., Martinez-Garcia, M., Hernández-Herrero, M. M., Gervilla, R., & Roig-Sagués, A. X. (2020). Effect of single and combined UV-C and ultra-high pressure homogenisation treatments on inactivation of Alicyclobacillus acidoterrestris spores in apple juice. *Innovative Food Science & Emerging Technologies, 60*, 102299. https://doi.org/10.1016/j.ifset.2020.102299

Sommer, R., Haider, T., Cabaj, A., Heidenreich, E., & Kundi, M. (1996). Increased inactivation of Saccharomyces cerevisiae by protraction of UV irradiation. *Applied and Environmental Microbiology, 62*(6), 1977–1983. https://doi.org/10.1128/aem.62.6.1977-1983.1996